*Materials Transactions*, Vol. 56, No. 10 (2015) pp. 1658 to 1663


# Strain Softening Induced by High Pressure Torsion in Copper Alloys

Yanzhao Pang[1,*1], Peng Li[1,*1], Hyoung Seop Kim[2], Yulan Gong[3], Yu Shen[1,*1], Lele Sun[1,*1] and Xinkun Zhu[1,*2]

[1]*Faculty of Materials Science and Engineering, Kunming University of Science and Technology, Kunming, Yunnan 650093, China*
[2]*Department of Materials Science and Engineering, Pohang University of Science and Technology, Pohang 790-784, Korea*
[3]*Faculty of Science, Kunming University of Science and Technology, Kunming, Yunnan 650093, China*

Three kinds of Cu-Al alloys and a pure Cu sample with different stacking fault energies (SFEs) are deformed using room temperature rolling (RR) and high pressure torsion (HPT), respectively. The microstructure is analysed by means of transaction electron microscopy and X-ray diffraction. It is found that HPT is more feasible to obtain nanocrystals and profuse twins. Tailoring the SFE can promote sample strength without sacrificing the ductility of the Cu alloys. The tensile properties of samples processed by HPT and RR are compared. It is discovered that the HPT process leads to the strain softening phenomenon in samples with relatively high SFE. The excellent mechanical properties can be obtained in samples deformed by HPT with a SFE of 6 mJ/m$^2$, in which strain softening was restrained and strain hardening played a dominant role in the deformation process. The relationship between tensile properties and microstructures of the deformed metals is also investigated.
[doi:10.2320/matertrans.MA201579]

(Received March 23, 2015; Accepted July 16, 2015; Published September 4, 2015)

***Keywords:*** *high-pressure torsion, stacking fault energy, strain softening, mechanical properties, microstructure*

## 1. Introduction

In recent years, there have been considerable interests in bulk ultrafine grain (UFG) or nanocrystalline (NC) materials due to their superior mechanical properties. Valiev *et al.* proposed the methods of severe plastic deformation (SPD) and elaborated the microstructural characteristics and mechanical and multi-functional properties of metallic materials processed by SPD.[1,2] High-pressure torsion (HPT) is more effective to modify microstructure and obtain NC than other SPD processes, because it is possible to exert extremely large plastic strain on samples. The HPT process can be used to obtain equiaxed grains, in which high-angle grain boundaries (HAGB) are the major part of the grain boundaries (GB). Therefore, HPT represents the excellent process for the creation of UFG or NC structure. Meanwhile, recent papers reported that HPT may lead to straining softening simultaneously grain refinement in already hardened NC Ni[3] as well as in some alloys such as Ni-Fe alloy,[4] Al-Zn alloy[5] and Zn-Al-Cu alloy.[6]

However, there are limitations of HPT in the small physical sample size and in the requirement of keeping a appropriate level of homogeneity between the edge and the center of the disc-shaped specimens.[7] Because the HPT samples are too small to be applied to tensile tests, the disk samples processed by HPT are sometimes rolled at room temperature to make them big enough or are machined for miniature tensile specimens.

As an important material parameter for plastic deformations, stacking fault energy (SFE) has a great influence on the deformation behaviors of metal materials. In addition, it is found that SFE also has a significant influence on the process of grain refinement in SPD.[8] SFE affects the microstructure and deformation behaviors because SFE controls probability of cross slip, which is a possible mechanism of dynamic recovery along with dislocation climb.[9–11] Another effect of SFE is the tendency to generate deformation twinning.[12] Deformation twinning is frequently observed in materials with low SFEs, such as Cu-Al alloys[13] and austenite stainless steels,[14] although they are processed at ambient temperature and fairly low strain rates. Thus, SFE has a great influence on the mechanical property of materials. Moreover, the strength and ductility of metals can be simultaneously promoted by decreasing SFE. The SFE value changes with solute element contents in alloys and temperature.

In order to further understand the importance of the SFE and the phenomenon of strain softening, this study seeks to elucidate the effects of the SFE and conditions of causing strain softening. This paper also explores the role of deformation routes in tensile properties and microstructure features of NC Cu–Al alloys with various SFEs processed by different SPD techniques.

## 2. Experiment Details

Cu-6.9 mass%Al, Cu–4.5 mass%Al and Cu–2.2 mass%Al alloys with SFEs of 6, 7 and 28 mJ/m$^2$, respectively, were prepared using induction vacuum melting.[13,15,16] For comparison, commercial pure copper with SFE of 78 mJ/m$^2$ was also prepared.[15] Before RR, pure Cu plates were annealed in vacuum at 873 K for 2 h and Cu-Al alloy plates were annealed in vacuum at 1023–1073 K for 4 h. Thus, some local defects were eliminated and the composition of these materials became more uniform after the annealing treatment. Then, we divided the homogenized samples into two groups. Samples in one group were rolled from the thickness of 7 mm to the final thickness of approximately 0.4 mm at room temperature. While those in the other were first rolled at room temperature from the thickness of 7 mm to approximately

*[1]Graduate Student, Kunming University of Science and Technology
*[2]Corresponding author, E-mail: xk_zhu@hotmail.com

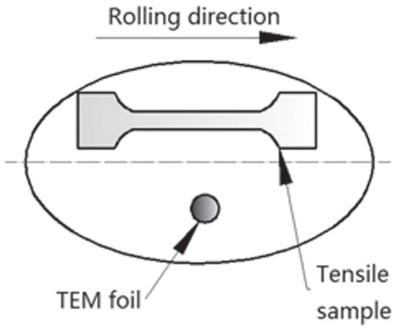


Fig. 1 Schematic illustration of the HPT and rolled sample showing the location for the tensile sample and TEM sample.

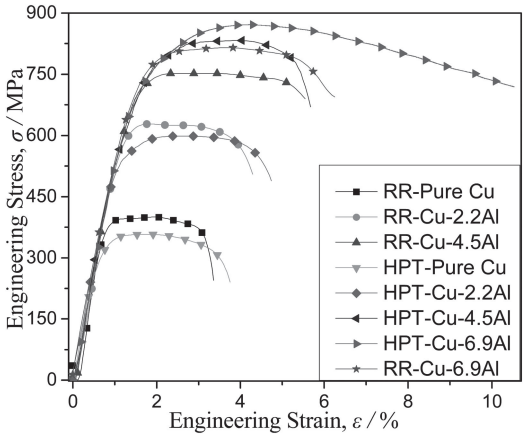


Fig. 2 Engineering stress-strain curve of samples processed by HPT and RR for pure Cu, Cu-2.2Al, Cu-4.5Al and Cu-6.9Al.

1 mm and then were sliced into small disks with diameters of about 20 mm. The HPT processing was carried out using a conventional facility, in which the disks were fixed between a rotational lower anvil and a stationary upper.[17] A total of five turns was applied to each disk at a rotation speed of 1 rotation/min, with an imposed pressure of 2.5 GPa at ambient temperature. Each disk had a thickness of ~0.5 mm after HPT. Following the HPT procedure, each disk was processed by RR to a final thickness of ~0.2 mm.

The typical RR tensile samples shaped in dog bone with a gauge width and length of 5 and 15 mm, respectively, were used to the tensile tests. As illustrated in Fig. 1, the HPT-processed tensile samples shaped in dog bone had a gauge width of 2 mm and a length of 12 mm oriented along the rolling direction. They were cut from position designated $0.5R$, where $R$ is the radius of the disk. At room temperature, a SHIMAZU Universal Tester machine was used to perform the tensile tests at a constant strain rate of $1 \times 10^{-4}\,s^{-1}$. More than three tensile tests were carried out for each kind of samples to ensure the reliability of the results.

Quantitative X-ray diffraction (XRD) analyses of the samples were carried out using a diffractometer with Cu $K_\alpha$ radiation, operating at 1.2 kW. Annealed pure silicon sheet with fully grown grains was used to remove the instrument broadening of XRD peak-broadening for calculating both the microstrain and the crystallite size. The $\theta$–$2\theta$ scans were implemented at ambient temperature to measure the twin density, dislocation density and lattice constant.

A FEI Tecnai $G^{-2}$ TF30 S-Twin transmission electron microscope (TEM) operated at 300 kV was used to investigate microstructure of the specimens. The TEM foils, with a diameters of 3 mm, were prepared on a TenuPol-5 twin jet polishing operated at a voltage of about 14 V, temperature of 295 K and flow rate of 40, with a solution of 50% distilled water, 25% ethyl alcohol and 25% phosphoric acid.

## 3. Experiment Results

For analysis of effects of SFE and processing routes on mechanical properties of the deformation-processed materials, stress-strain curves obtained by uniaxial tensile tests were compared for all samples. As shown in Fig. 2, the results exhibit that the tensile properties are influenced by both SFE and processing route selected. The decrease of SFE contributes to increase in the strength and ductility simultaneously in both HPT and RR groups. The HPT-processed sample of Cu–6.9Al exhibits higher yield strength (YS) and larger uniform elongation (UE), meaning a combination of higher strength and better ductility, compared to those of the RR-processed counterparts. Meanwhile, the HPT-processed samples of the pure Cu and Cu–2.2Al have lower values of strength but larger UE and elongation to failure compared to those of the RR-processed counterparts.

For further understanding of mechanical performances, the strain hardening of the samples was analyzed. The strain hardening rate $\theta$, can be defined by the following expression:[18]

$$\theta = (\partial\sigma/\partial\varepsilon)_{\dot{\varepsilon}} \tag{1}$$

where $\varepsilon$ is the true strain, $\sigma$ is the true stress and $\dot{\varepsilon}$ is the strain rate. The normalized work hardening rate $\theta$ of each sample was shown in Fig. 3(a) and Fig. 3(b). The Cu–6.9Al samples have the highest capacity for strain hardening among these samples. These results clearly indicate that the strain hardening rate $\theta$ of both the HPT and RR samples increase with a decrease in SFE. It means that the better ductility can be obtained in samples with lower SFE. The work hardening rate curves also suggest that the dynamic recovery can be delayed in samples with lower SFE.

The twin density $\beta$ and the dislocation density $\rho$, as two important parameters to describe the microstructure, can be measured by the XRD analysis. The average crystallite size $d_{XRD}$ and the microstrain ($\langle\varepsilon^2\rangle^{1/2}$) can be estimated from the Scherrer-Wilson method through the pairs of (111)-(222) and (200)-(400) reflection by the XRD peak broadening. The average dislocation density $\rho$ can be deduced from average grain size $d$ and microstrain ($\langle\varepsilon^2\rangle^{1/2}$) according to the following relationship:[19–21]

$$\rho = 2\sqrt{3}\langle\varepsilon^2\rangle^{1/2}/d_{XRD}b, \tag{2}$$

where $b$ is the Burgers vector, $b = (\sqrt{2}/2)a$, and $a$ is the lattice parameter for each kind of sample. The twin density $\beta$ is defined as the probability of detecting a twin boundary between any two neighboring {111} planes. It can be calculated based on the equation:[22,23]

$$\beta = [\Delta C \cdot G \cdot (2\theta)_{111} - \Delta C \cdot G \cdot (2\theta)_{200}] / (11\tan\theta_{111} + 14.6\tan\theta_{200}), \tag{3}$$

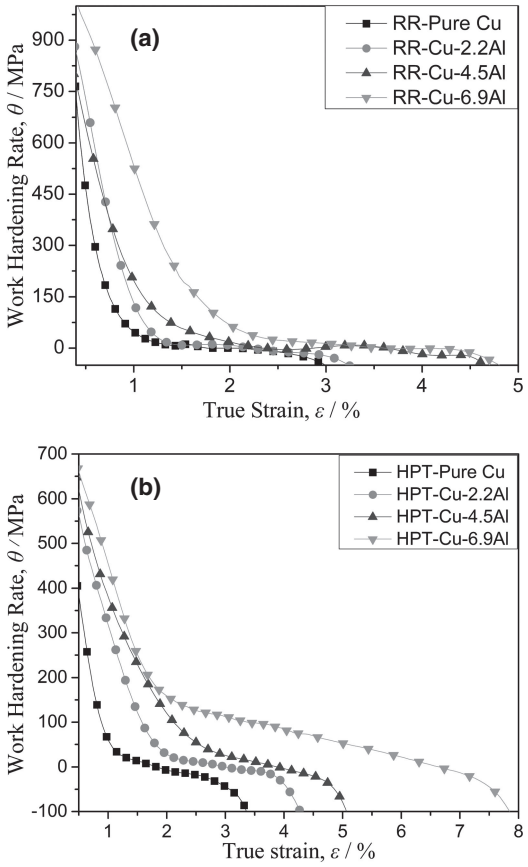


Fig. 3 The normalized work hardening rate $\theta$, against the true strain $\varepsilon$, of Cu-Al alloys. (a) deformed by rolling at room temperature and (b) deformed by HPT then rolled at room temperature.

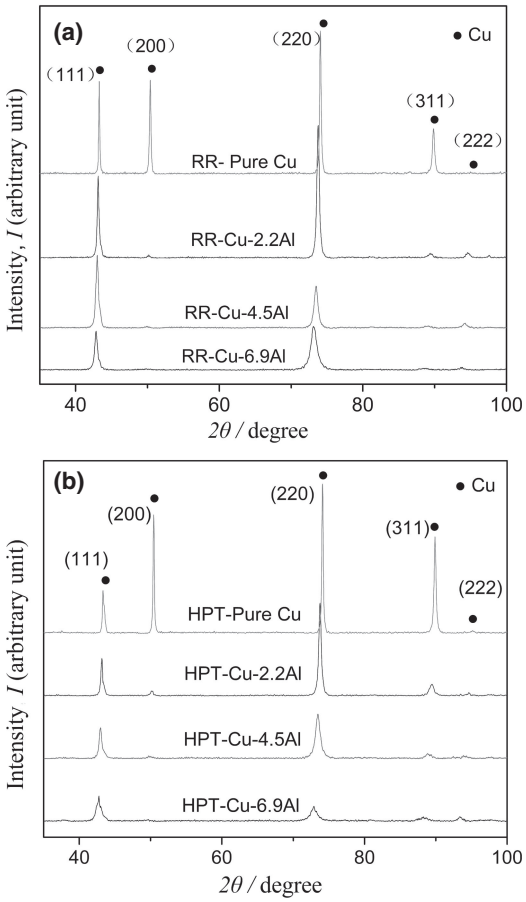


Fig. 4 XRD patterns of samples for Cu-Al alloys and pure Cu. (a) deformed by RR and (b) deformed by HPT.

where $\Delta C \cdot G \cdot (2\theta)_{200}$ and $\Delta C \cdot G \cdot (2\theta)_{111}$ are the absolute angular deviations of the peak summit from the gravity center of the {200} and {111} diffraction peaks of XRD, respectively. The XRD patterns of these samples are presented in Fig. 4, indicating an increased peak broadening with decreasing SFE. Then, the microstrains and the average grain sizes of the HPT- and RR-processed samples are presented in Fig. 5(a). These grain size values of different kinds of samples can be compared if they are estimated with the same measuring error and under the same operation condition. The crystallite size of the samples decreases, while the microstrain increases, with decreasing the SFE. These results show that SFE plays a significant role in the grain refinement process. Furthermore, the grain size of the RR-processed samples is always larger than that of the HPT-processed counterparts. Figure 5(b) presents that the dislocation density and twin density increase with reducing SFE. In particular, their densities increase much faster when the SFE is lower than 28 $mJ/m^2$. The increments of dislocation density for HPT-processed samples are much larger than those of RR-processed counterparts, with SFE reducing from 28 $mJ/m^2$ to 6 $mJ/m^2$. That is to say, the HPT-processed samples are more likely to accumulate dislocation with decreasing SFE. Moreover, the twin density of the HPT-processed samples is larger than that of RR-processed counterparts, as shown in Fig. 5(b). The microstructure of both HPT- and RR-processed samples for Cu-4.5Al are presented in Fig. 6. It shows that more deformation twins appear in the HPT-processed sample for Cu-4.5Al than in the RR counterpart.

## 4. Analysis and Discussion

### 4.1 The effect of SFE on microstructure and mechanical properties

As an intrinsic material parameter, the SFE plays an important part in the microstructure evolution and grain subdivision. It has been confirmed that in materials with medium or high SFE, the process of grain refinement is dominated by dislocation activities during plastic deformation. On the other hand, for metals with low SFE, dislocation subdivision and twin fragmentation dominate the grain refinement.[24–27] With reducing SFE, a wide stacking fault ribbon, which hinders whole dislocations to climb and cross-slip, contributes to the separation of a perfect dislocations into two partial dislocations. It is hard for partial dislocations to migrate in the form of cross-slip. Hence, the requirement for twinning stress becomes easier to meet in low SFE materials than that of the stress for the motion of the partial dislocations. Therefore deformation twins form, as shown in Fig. 6. In other words, a lower SFE makes it easier to form deformation twins. Furthermore, profuse twin boundaries (TBs) induced by lowering SFE can not only hinder the motion of dislocation, but act as locations for dislocation

storing.[28] Thus, the high dislocation density appears along with high twin density by reducing SFE in most cases. Hence, the interaction of these TBs and GBs dominants the grain refining process. It is consistent with the experimental result of XRD, in that lowering SFE causes grain refinement with an increase in defect (stacking faults, TBs and dislocations) densities during plastic deformation.

The interaction of dislocation-dislocation, twin-dislocation and twin–twin contributed by lowering SFE can greatly improve the flow stress. The high YS follows the improved flow stress. It is consistent with results of previous studies.[29–34] Besides, as mentioned above, due to the reduced SFE, the finer grain sizes appear and the strength increases, i.e. Hall-Petch strengthening. The addition of aluminum atoms not only lowers the SFE, but also leads to solution hardening, which improves the strength of the Cu-Al alloy. Despite the existence of solid solution hardening is unavoidable, the influence of solution strengthening is secondary.[35] Furthermore, dynamic recovery can be restrained through abundant TBs and wide stacking faults with the effects of segmenting dislocations. Further, the strain hardening rate can be improved by restraining dynamic recovery. The improved strain hardening rate can observably delay plastic instability and enhance the ductility.[32,36] Thus, the strength and ductility can be simultaneously enhanced by reducing the SFE in Cu-Al alloys. This is accordant with the research of An *et al.*[37] It is beyond dispute that Cu–6.9Al with the lowest SFE has the highest strength and the best ductility, namely, the optimal mechanical properties, as shown in Fig. 2.

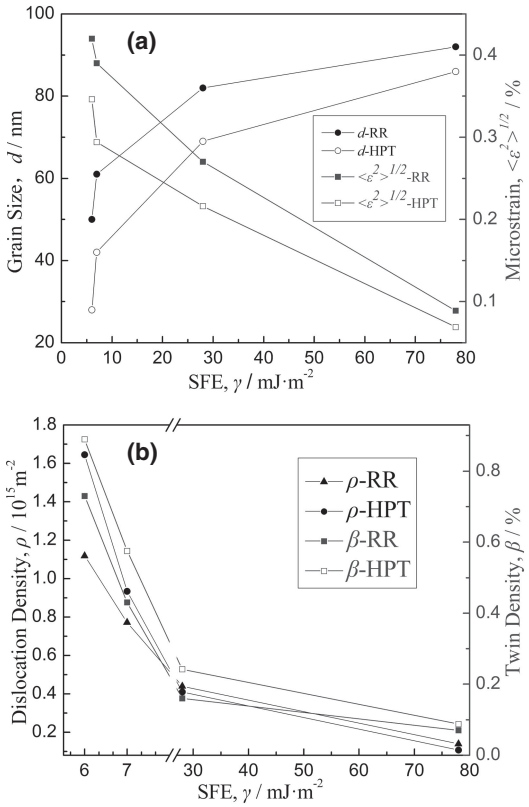


Fig. 5 Microstructure parameters of pure Cu and Cu-Al alloys against SFEs processed by HPT and RR. (a) microstrain $\langle\varepsilon^2\rangle^{1/2}$ and average grain size $d$ and (b) twin density $\beta$ and dislocation density $\rho$.

### 4.2 The effect of plastic strain

Plastic strain is always a key factor in the SPD processes. In the RR process, the true strain is defined as $\varepsilon = \ln(L_0/L_f)$, where $L_f$ and $L_0$ are the final and initial thicknesses of the workpiece plates, respectively.[38] Thus, in the current study, the strain $\varepsilon$ of the RR samples is approximate 2.98. While, during the HPT process, the equivalent true strain is defined as $\varepsilon_{HPT} = \ln(1 + \frac{2\pi Nr}{\sqrt{3}h})$, where $h$ is the disk thickness, $r$ is the distance from the torsion axes and $N$ is number of revolutions.[39] Therefore, the total strain can be calculated by $\varepsilon = \varepsilon_{r1} + \varepsilon_{HPT} + \varepsilon_{r2}$ in the HPT-processed samples, where $\varepsilon_{r1}$ is the strain of the HPT-processed samples deformed by rolling before HPT, $\varepsilon_{HPT}$ is the strain of the HPT-processed samples processed during HPT, and $\varepsilon_{r2}$ is the strain of the samples deformed by rolling after the HPT process. The total strain value $\varepsilon$ in the rim of the HPT-processed disks is about 8.84, which is almost three times larger than that of the RR-processed samples. The total true strain value of the HPT tensile samples is about 7.38.

Therefore, finer grain size and more twins can be obtained in HPT-processed samples. Strain softening is shown by

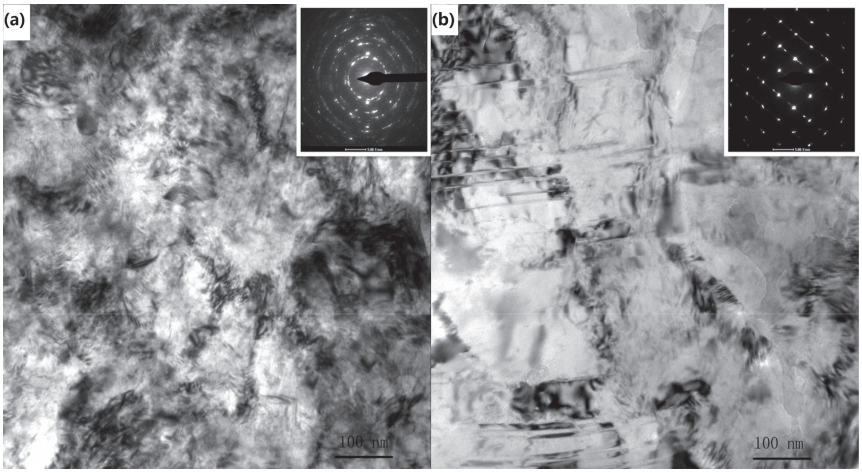


Fig. 6 Bright-field TEM micrographs and corresponding SAED pattern showing the microstructures processed by RR and HPT for Cu-4.5Al. (a) deformed by RR and (b) deformed by HPT.

comparing the stress-strain curves of the RR- and HPT-processed pure copper and Cu-2.2Al in Fig. 2. Liao *et al.* had also found the strain softening in NC Ni–Fe alloy induced by HPT.[4] The strain softening is owe to the reduction in the dislocation and grain growth. Mecking *et al.* proposed that the rate of change in the dislocation density dominates the plastic deformation of samples with high SFE.[40] Two prime competing parts simultaneously control the change of the dislocation. One is softening part (dynamic recovery) along with dislocation annihilation processes. The other is hardening part (dislocation storage). Besides, dynamic recovery is dominated by thermal activation, which is related to temperature and strain rate, and so on.[41]

With larger strain, the phenomenon of local adiabatic heating may take place in the pure Cu and Cu-2.2Al samples during the HPT process: both of them have high or medium SFE. Local adiabatic heating can not only cause dynamic recovery during HPT process, but also lead to a self-annealing within a several hours after the HPT processing.[42] Thus, the reduction in dislocation density and relaxation of residual stress can take place in the HPT-processed samples. A slight growth in grain size may also occur because dislocation annihilation and absorption at boundaries take place in the final stage of the HPT process, in which dynamic recovery is prior to dislocation storage. These analyses explain that the densities of defects (dislocation, vacancy) and the values of microstrains in the pure Cu and Cu-2.2Al samples during the HPT process are lower than those in the RR-processed counterparts, as shown in Fig. 4(b). The results agree well with the earlier studies.[43] Therefore, higher defects density in RR-processed samples with relatively high SFE could contribute to a higher strength, in comparison with the HPT-processed counterparts. Meanwhile, the profuse TBs and abundant stacking faults in Cu-4.5Al samples with low SFE can effectively suppress dynamic recovery during HPT process. This is consistent with earlier studies as well.[44] Hence, the rate of dislocation annihilation is slower than the rate of dislocation accumulation, and the hardening part (dislocation storage) dominants the plastic deformation. Thus, the highest strength could be achieved in samples with lowest SFE deformed by HPT with the profuse twins and highest defect densities.

## 5. Conclusion

(1) With decreasing SFE, wide stacking faults and profuse TBs increase the difficulty in cross-slip. Hence, dynamic recovery can be delayed in Cu-Al alloys with low SFE.
(2) SFE plays a key role in the mechanical properties of Cu-Al alloys. The current study shows that strength and ductility of Cu-Al alloys can be synergistically enhanced by tailoring the SFE.
(3) With larger strain, HPT is more effective to refine the grain size and increase twin densities than RR.
(4) Finally, the HPT technique leads to the phenomenon of strain softening for specimens with SFE higher than 28 $mJ/m^2$, in which dynamic recovery is more remarkable during the plasticity deformation. And strain softening is restrained in specimens with SFE lower than 7 $mJ/m^2$, which present the excellent mechanical properties.

## Acknowledgement

The authors would like to acknowledge financial supports by the National Natural Science Foundation of China (NSFC), Grant NO. 50874056, and the introduction of talents fund project of Kunming University of Science and Technology (grant KKSY201407100).

## REFERENCES

1) R. Z. Valiev and I. V. Alexandrov: Ann. Chim. **27** (2002) 3–14.
2) K. Kaneko, T. Hata, T. Tokunaga and Z. Horita: Mater. Trans. **50** (2009) 76–81.
3) X. Z. Liao, A. R. Kilmametov, R. Z. Valiev, H. Gao, X. Li, A. K. Mukherjee, J. F. Bingert and Y. T. Zhu: Appl. Phys. Lett. **88** (2006) 021909.
4) S. Ni, Y. B. Wang, X. Z. Liao, R. B. Figueiredo, H. Q. Li, Y. H. Zhao, E. J. Lavernia, S. P. Ringere, T. G. Langdon and Y. T. Zhu: Mater. Sci. Eng. A **528** (2011) 4807–4811.
5) A. Alhamidi, K. Edalati, Z. Horita, S. Hirosawa, K. Matsuda and D. Terada: Mater. Sci. Eng. A **610** (2014) 17–27.
6) M. Kawasaki, B. Ahn and T. G. Langdon: Mater. Sci. Eng. A **527** (2010) 7008–7016.
7) J. Wongsa-Ngam, M. Kawasaki and T. G. Langdon: J. Mater. Sci. **48** (2013) 4653–4660.
8) Y. H. Zhao, Y. T. Zhu, X. Z. Liao, Z. Horita and T. G. Langdon: Appl. Phys. Lett. **89** (2006) 121906.
9) S. M. Sivakumar and M. Ortiz: Comp. Meth. Appl. Mech. Eng. **193** (2004) 5177–5194.
10) K. Youssef, M. Sakaliyska, H. Bahmanpour, R. Scattergood and C. Koch: Acta Mater. **59** (2011) 5758–5764.
11) Z. Hegedűs, J. Gubicza, M. Kawasaki, N. Q. Chinh, Z. Fogarassy and T. G. Langdon: Mater. Sci. Forum **729** (2012) 222–227.
12) P. Müllner and C. Solenthaler: Mater. Sci. Eng. A **230** (1997) 107–115.
13) S. Qu, X. H. An, H. J. Yang, C. X. Huang, G. Yang, S. Q. Zang, G. Z. Wang, D. S. Wu and Z. F. Zhang: Acta Mater. **57** (2009) 1586–1601.
14) S. Vercammen, B. Blanpain, B. C. De Cooman and P. Wollants: Acta Mater. **52** (2004) 2005–2012.
15) A. Rohatgi, K. S. Vecchio and G. T. Gray, III: Metall. Mater. Trans. A **32** (2001) 135–145.
16) P. C. J. Gallagher: Metall. Trans. **1** (1970) 2429–2461.
17) K. S. Ghosh, N. Gao and M. J. Starink: Mater. Sci. Eng. A **552** (2012) 164–171.
18) C. C. Koch, D. G. Morris, K. Lu and A. Inoue: MRS Bull. **24** (1999) 54–58.
19) Y. H. Zhao, X. Z. Liao, Z. Jin, R. Z. Valiev and Y. T. Zhu: Acta Mater. **52** (2004) 4589–4599.
20) G. K. Williamson and R. E. Smallman: Philos. Mag. **1** (1956) 34–46.
21) R. E. Smallman and K. H. Westmacott: Philos. Mag. **2** (1957) 669–683.
22) C. X. Huang, W. P. Hu, Q. Y. Wang, C. Wang, G. Yang and Y. T. Zhu: Mater. Res. Lett. **3** (2015) 88–94.
23) C. N. J. Wagner: Acta Metal. **5** (1957) 427–434.
24) L. Balogh, T. Ungár, Y. Zhao, Y. T. Zhu, Z. Horita, C. Xu and T. G. Langdon: Acta Mater. **56** (2008) 809–820.
25) Y. T. Zhu and T. C. Lowe: Mater. Sci. Eng. A **291** (2000) 46–53.
26) Y. B. Wang, X. Z. Liao, Y. H. Zhao, E. J. Lavernia, S. P. Ringer, Z. Horita, T. G. Langdon and Y. T. Zhu: Mater. Sci. Eng. A **527** (2010) 4959–4966.
27) C. X. Huang, W. Hu, G. Yang, Z. F. Zhang, S. D. Wu, Q. Y. Wang and G. Gottstein: Mater. Sci. Eng. A **556** (2012) 638–647.
28) J. Gubicza, N. Q. Chinh, J. L. Lábár, Z. Hegedus and T. G. Langdon: Mater. Sci. Eng. A **527** (2010) 752–760.
29) Z. W. Wang, Y. B. Wang, X. Z. Liao, Y. H. Zhao, E. J. Lavernia, Y. T. Zhu, Z. Horita and T. G. Langdon: Scr. Mater. **60** (2009) 52–55.
30) Y. H. Zhao, Z. Horita, T. G. Langdon and Y. T. Zhu: Mater. Sci. Eng. A **474** (2008) 342–347.

31) K. Lu, L. Lu and S. Suresh: Science **324** (2009) 349–352.
32) X. H. An, W. Z. Han, C. X. Huang, P. Zhang, G. Yang, S. D. Wu and Z. F. Zhang: Appl. Phys. Lett. **92** (2008) 201915.
33) Y. S. Li, Y. Zhang, N. R. Tao and K. Lu: Acta Mater. **57** (2009) 761–772.
34) Y. H. Zhao, X. Z. Liao, Z. Horita, T. G. Langdon and Y. T. Zhu: Mater. Sci. Eng. A **493** (2008) 123–129.
35) V. S. Sarma, J. Wang, W. W. Jian, A. Kauffmann, H. Conrad, J. Freudenberger and Y. T. Zhu: Mater. Sci. Eng. A **527** (2010) 7624–7630.
36) L. Lu, T. Zhu, Y. Shen, M. Dao, K. Lu and S. Suresh: Acta Mater. **57** (2009) 5165–5173.
37) X. H. An, Q. Y. Lin, S. D. Wu, Z. F. Zhang, R. B. Figueiredo, N. Gao and T. G. Langdon: Scr. Mater. **64** (2011) 954–957.
38) S. Nagarjuna, U. Chinta Babu and P. Ghosal: Mater. Sci. Eng. A **491** (2008) 331–337.
39) A. P. Zhilyaev and T. G. Langdon: Prog. Mater. Sci. **53** (2008) 893–979.
40) H. Mecking and U. F. Kocks: Acta Metal. **29** (1981) 1865–1875.
41) F. R. N. Nabarro: Acta Metal. **37** (1989) 1521–1546.
42) S. Scheriau, M. Kriegisch, S. Kleber, N. Mehboob, R. Grössinger and R. Pippan: J. Mag. Mag. Mater. **322** (2010) 2984–2988.
43) S. Ni, Y. B. Wang, X. Z. Liao, S. N. Alhajeri, H. Q. Li, Y. H. Zhao, E. J. Lavernia, S. P. Ringer, T. G. Langdon and Y. T. Zhu: Mater. Sci. Eng. A **528** (2011) 3398–3403.
44) X. H. An, S. Qu, S. D. Wu and Z. F. Zhang: J. Mater. Res. **26** (2011) 407–415.